REPORT DOCUMENTATION PAGE

Form Approved
OMB No. 0704-0188

1. REPORT DATE *(DD-MM-YYYY)*	2. REPORT TYPE	3. DATES COVERED *(From - To)*
08-06-2006	Journal article (refereed)	

4. TITLE AND SUBTITLE	5a. CONTRACT NUMBER
Observed Deep Circulation in the Ulleung Basin	
	5b. GRANT NUMBER
	5c. PROGRAM ELEMENT NUMBER PE0601153N

6. AUTHOR(S)	5d. PROJECT NUMBER
W.J. Teague, K.L. Tracey, D.R. Watts, J.W. Book, K.I. CHange, P.J. Hogan, D.A. Mitchell, M.S. Suk, M. Wimbush, J.H. Yoon	
	5e. TASK NUMBER
	5f. WORK UNIT NUMBER 73-7507-02-5

7. PERFORMING ORGANIZATION NAME(S) AND ADDRESS(ES)	8. PERFORMING ORGANIZATION REPORT NUMBER
Naval Research Laboratory Oceanography Division Stennis Space Center, MS 39529-5004	NRL/JA/7330-02-61

9. SPONSORING/MONITORING AGENCY NAME(S) AND ADDRESS(ES)	10. SPONSOR/MONITOR'S ACRONYM(S)
Office of Naval Research 800 N. Quincy St. Arlington, VA 22217-5660	ONR
	11. SPONSOR/MONITOR'S REPORT NUMBER(S)

12. DISTRIBUTION/AVAILABILITY STATEMENT
Approved for public release, distribution is unlimited.

13. SUPPLEMENTARY NOTES

14. ABSTRACT
Records from 16 current meters and 23 pressure gauges moored near the sea floor in the Ulleung Basin of the southwestern Japan/East Sea (JES) characterized the deep circulation between June 1999 and July 2001. Mean currents range from 1 to 4 cm/s and deep pressure anomalies range from 3 to 10 mbar, with horizontal correlation scales of about 40 km, and with integral time scales that range from about 5 to 20 days. Focusing here on the 90-day to interannual variability, synoptic maps of the deep currents and dynamic pressure fields determine that the deep circulation in the Ulleung Basin is cyclonic, with additional multiple cyclonic and anticyclonic cells that occur on sub-basin spatial scales. Over the Korea Plateau a northward deep outflow is observed that suggests an anticyclonic circulation pattern to the north. The annual average deep currents are remarkably similar for the 2 years, only slightly weaker in the 2nd year. No seasonal pattern is discernible, except weakly at one or two sites.

15. SUBJECT TERMS
Ulleung Basin; Japan/East Sea; circulation; cyclonic

16. SECURITY CLASSIFICATION OF:			17. LIMITATION OF ABSTRACT	18. NUMBER OF PAGES	19a. NAME OF RESPONSIBLE PERSON
a. REPORT	b. ABSTRACT	c. THIS PAGE	UL	25	William J. Teague
Unclassified	Unclassified	Unclassified			**19b. TELEPHONE NUMBER** *(Include area code)* (228) 688-4734

Observed deep circulation in the Ulleung Basin

W.J. Teague[a,*], K.L. Tracey[b], D.R. Watts[b], J.W. Book[a], K.-I. Chang[c],
P.J. Hogan[a], D.A. Mitchell[b], M.-S. Suk[c], M. Wimbush[b], J.-H. Yoon[d]

[a]*Naval Research Laboratory, Stennis Space Center, MS 39529-5004, USA*
[b]*GSO, University of Rhode Island, Narragansett, RI 02882-1197, USA*
[c]*Korea Ocean Research and Development Institute, Seoul, Korea*
[d]*Research Inst. Applied Mech., Kyushu University, Fukuoka, Japan*

Abstract

Records from 16 current meters and 23 pressure gauges moored near the sea floor in the Ulleung Basin of the southwestern Japan/East Sea (JES) characterized the deep circulation between June 1999 and July 2001. Mean currents range from 1 to 4 cm/s and deep pressure anomalies range from 3 to 10 mbar, with horizontal correlation scales of about 40 km, and with integral time scales that range from about 5 to 20 days. Focusing here on the 90-day to interannual variability, synoptic maps of the deep currents and dynamic pressure fields determine that the deep circulation in the Ulleung Basin is cyclonic, with additional multiple cyclonic and anticyclonic cells that occur on sub-basin spatial scales. Over the Korea Plateau a northward deep outflow is observed that suggests an anticyclonic circulation pattern to the north. The annual average deep currents are remarkably similar for the 2 years, only slightly weaker in the second year. No seasonal pattern is discernable, except weakly at one or two sites.
Published by Elsevier Ltd.

1. Introduction

In the Ulleung Basin (UB) at depths from about 400 m to the bottom (2200 m), the density is essentially uniform with temperatures less than 1 °C and salinities less than 34.1 psu (Kim et al., 1991; Chang et al., 2002). This nearly homoge-

neous deep water is referred to as the East (or Japan) Sea Proper Water (ESPW). These deep waters do not originate by local convection in the UB since surface temperatures in winter exceed 8 °C, nor by inflow through the Korea/Tsushima Strait since the sill depth is less than 200 m. Instead, ESPW is believed to form in winter by sinking along the Russian shelf break in the northwestern JES (Vasilev and Makashin, 1992; Senjyu and Sudo, 1994) and by convection to depths of about 1000 m in the deep (almost 4000 m

*Corresponding author. Tel.: +1 228 688 4734;
fax: +1 228 688 5997.
E-mail address: teague@nrlssc.navy.mil (W.J. Teague).

in depth) central Japan Basin (Seung and Yoon, 1995; Senjyu and Sudo, 1993, 1996; Choi, 1996). The cold bottom water is believed to enter the UB through the deep channel between Ulleung and Dok Islands (Kim et al., 1991) or over the Korea Plateau (KP) (Cho and Kim, 1995; Shin et al., 1998).

The distinctive properties of the deep water require at least some weak deep circulation to maintain its homogeneity. The absence of stratification suggests negligible vertical shear at geostrophic length and time scales. Few direct measurements of the deep flows exist in the JES to confirm this, however. The earliest measurements of the deep flow were made in the Japan Basin. Nanniti et al. (1966) used a drifting float at 800 m depth to observe a drift of 1.5 cm/s. The first long-term moored measurements of the mid-depth and deep currents were made by Takematsu et al. (1999) as part of the CREAMS (Circulation Research of East Asian Marginal Seas) program. They found energetic deep eddy currents in the Japan Basin, with speeds of the order of 10 cm/s between 900 and 2400 m, observed to be vertically coherent and nearly depth independent. They also reported a pronounced seasonal pattern, with strong currents in March and April and weak currents in the summer.

In the Ulleung Basin, long-term measurements of currents have been more difficult to make because of intense fishing, in which crabbers lay long lines of crab traps (1 km and longer) on the bottom at depths in excess of 1000 m. A mooring deployed by Lie et al. (1989) for about 2.5 months in water depth of 800–900 m off the east coast of Korea observed southwestward flow with a mean of 3.8 cm/s at 790 m depth and peak speeds of 11 cm/s. Recently, Chang et al. (2002) reported substantial southward flow averaging over 6 cm/s at about 1200 m depth with a mooring deployed near 37°N along the Korean slope and maintained for about 2 years. They were the first to measure mid-depth and near-bottom velocities in the interior of the UB. Since 1996, they have maintained a single current meter mooring with several levels instrumented in the deep channel (Ulleung Interplain Gap, UIG) between Ulleung Island and Dok Island. In addition, since 1998 two moorings,

each with a single deep current meter, have been deployed in the southern and central portions of the UB. The subthermocline currents were nearly depth-independent, with bottom velocities averaging 1–2 cm/s.

Because of the paucity of direct observations, the general circulation in the Ulleung Basin has remained poorly understood and theories conflict even regarding the cyclonic or anticyclonic sense of the mean flow. Water mass evidence suggests that the deep waters come from the Japan Basin. These waters can only enter the Ulleung Basin via the UIG or over the Korea Plateau between the Korean coast and Ulleung Island (Fig. 1). Kim et al. (1991) suggested that the anticyclonic circulation observed in the upper layer with CTD data would extend to the bottom as well due to the uniform density below the thermocline. In contrast, the recent current measurements at four sites made by Chang et al. (2002) indicate a cyclonic deep-circulation pattern in the UB.

To elucidate the near-surface and bottom circulation patterns in the Ulleung Basin an observational program was recently conducted by the University of Rhode Island (URI) and the Naval Research Laboratory as part of the United States' JES program. The deep current measurements in this program are the most comprehensive ever made in the JES. Data are obtained from an array of 11 recording current meter (RCM) moorings and 23 pressure-sensor-equipped inverted echo sounders (PIES) deployed for 2 years beginning in June 1999 (Fig. 1). The current meter moorings are coordinated with the set of four current meter moorings deployed by the Korean Ocean Research and Development Institute (KORDI) and presented in Chang et al. (2002). An additional mooring in the southeastern portion of the UB was deployed by the Research Institute of Applied Mechanics (RIAM) of Kyushu University. Altogether, 16 RCM sites are used to level the pressure measurements, and the combined datasets generate daily regional maps of the deep stream function and the deep current patterns. This paper provides a thorough description of the mean deep currents and their longer than 90-d-period variability, as observed by this highly instrumented array.
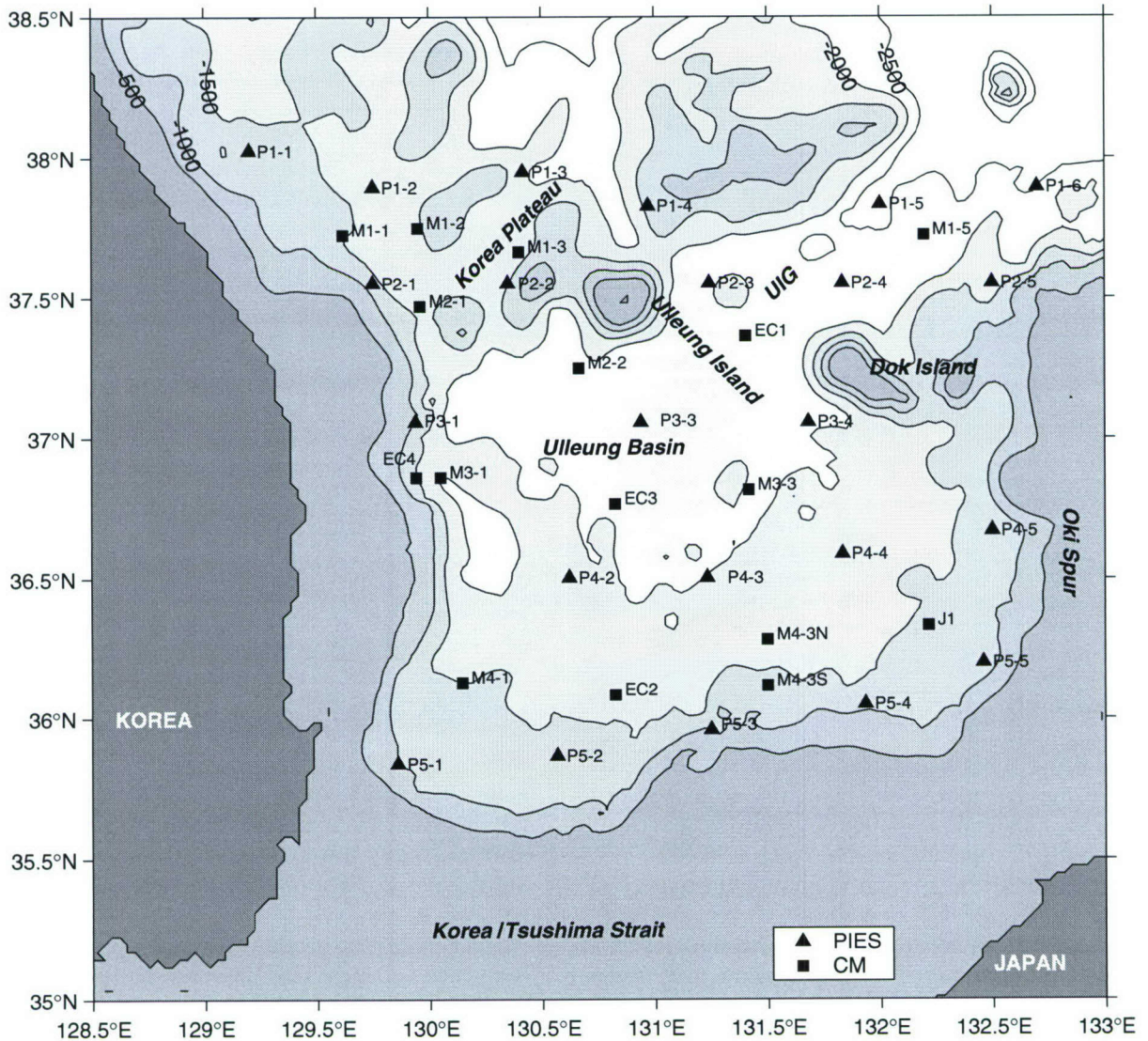
Fig. 1. Locations of the current meter moorings (squares) and PIES (triangles) are shown. The current meter moorings consist of 11 from URI (M moorings), four from KORDI (E moorings), and one from RIAM (J mooring). All PIES (P moorings) are from URI. Depths are in meters. UIG denotes the Ulleung Interplain Gap.

2. Data processing

2.1. Current meter records

We used Aanderaa RCM8 current meters standardly equipped with a rotor and vane for speed and direction measurements. Geographic positions, instrument depths, bottom depths, and deployment times of the moorings are listed in Table 1. All of the current meters are located 20–30 m above the bottom in water depths ranging from about 1200 to over 2000 m. URI RCMs recorded at nominal 1-h intervals during the 2-year deployment period. Due to instrument failures at sites M4-3S and at M3-3, their data returns were limited to about a year and to 2 months,

Table 1
Current meter summary

Mooring	Lat	Lon	Depth	Bottom	Day1	Day2	Stall %
M1-1	37.72	129.62	1197.	1220.	160.	910.	14
M1-2	37.75	129.95	1639.	1662.	160.	846.	18
M1-3	37.66	130.40	1547.	1570.	161.	913.	64
M1-5	37.72	132.20	2425.	2448.	163.	904.	35
M2-1	37.47	129.96	1534.	1557.	162.	912.	39
M2-2	37.25	130.67	2207.	2227.	195.	911.	17
M3-1	36.86	130.05	2188.	2211.	162.	914.	22
M3-3	36.82	131.42	2028.	2051.	159.	226.	46
M4-1	36.13	130.15	1527.	1550.	157.	909.	17
M4-3	36.28	131.50	1774.	1797.	164.	908.	11
M4-3	36.12	131.50	1523.	1546.	158.	533.	13
EC1	37.37	131.40	2355.	2375.	145.	950.	47
EC2	36.08	130.83	1650.	1670.	143.	830.	47
EC3	36.77	130.83	2194.	2220.	144.	833.	42
EC4	36.87	129.95	1228.	1250.	146.	833.	13
J1	36.35	132.13	1383.	1410.	170.	887.	33

Latitude (Lat), longitude (Lon), current meter depth (Depth), bottom depth (Bottom), deployment times (start time of Day1 and end time of Day2 relative to January 1, 1999), and percentage of stall time (Stall %) are provided.

respectively. At site M1-3 the rotor stopped spinning for about 9 months half-way through the deployment period; however, it rotated unimpeded and produced an apparently normal record for the final 3 months. The KORDI RCM records are fully documented by Chang et al. (2002).

The RCM8 registers a minimum current speed of 1.1 cm/s, which is treated as a current stall (i.e., zero speed); thus current speeds less that 1.1 cm/s are indistinguishable. We chose to use zero speed rather than use, for example, half the stall speed because the direction measurement becomes unreliable at low current speeds. Since the resolution of the RCM8 is about 0.3 cm/s, the minimum resolvable current speed is 1.4 cm/s. On occasion, some of the records contained unrealizably high or low speeds. These values are also treated as stalls in the data processing steps. The speed and direction records are converted into u and v velocity component time series, respectively positive towards the east and the north.

In the next processing step, the eight main tidal constituents (M2, S2, N2, K2, K1, O1, Q1, and P1) are removed. A harmonic analysis technique is used for determining the constituent amplitude and phase by least-squares fitting sinusoids to the raw data. This procedure advantageously operates without equally spaced data and thus can skip over the stall periods. By the Rayleigh criterion, in a low-noise environment the tide constituents, M2, S2, N2, K1, O1, and Q1, can be resolved with 1 month of data, while 6 months of data are needed for the additional resolution required by K2 and P1. Thus, the URI RCM record lengths are more than adequate to resolve the tides. In general, tidal amplitudes in the UB are less than 40 cm and the tidal currents account for a low percentage of the total current variability.

After removal of the tidal signals from both velocity components, splines are fitted individually to the u and v time series specifying knots at all non-stall values. For periods that contain no more than five consecutive stalls (nominally 5 h), the stalls are replaced with spline-fitted values. For consecutive stalls extending for longer periods, u and v are set to zero. Table 1 also lists the percentage of time with zero current remaining in the records (Stall %) after the short stall periods have been interpolated.

Of the 11 URI RCMs, 10 instruments exhibited clock drifts of 18–24 min and one clock drifted about 38 min. The time base of each current record was adjusted by spreading the appropriate clock drift uniformly through the entire current record. Subsequently, the u and v data were interpolated onto 1-h intervals.

Since analyses in this paper focus on lower frequencies, the current data are presented after low-pass filtering using a 40-h cutoff filter. This filtering has removed tidal and inertial currents, which contain periods of about 20 h at these latitudes, and which are a dominant source of short-period variability in all of the records.

2.2. Pressure records

Pressure is measured with Digiquartz pressure transducers (models 46K-101 and 410K-101) manufactured by Paroscientific, Inc. Paros (1976) and Wearn and Larson (1982) provide detailed descriptions of these transducers. They are mounted on inverted echo sounders (IES models 4 and 5 used in this experiment), which were

tethered less than 1 m above the seafloor. A description of the IES and mooring configuration is provided in Chaplin and Watts (1984). The pressure sensors have a resolution of 0.1 mbar (1 mbar = 1 hPa) and an absolute accuracy of 10–30 mbar. The processing of the individual pressure records from initial editing through low-pass filtering is described in Mitchell et al. (2005). Summarizing briefly, the initial processing involved removal of jumps and long-term drifts. Abrupt jumps (offsets) ranging in magnitude from a few centimeters to tens of meters occurred at 11 sites. Jumps like this had not been observed in previous experiments using the same sensors, and in this case they have been attributed to the instruments being jostled by crab fishermen. Because corresponding jumps also were observed in the travel-time records, the pressure jumps are readily identified and removed. Most of the instruments exhibited drifts less than 25 mbar over the 2-year period. However large drifts (200–450 mbar) occurred in five of the records, which were from a common batch of older gauges (these have subsequently been retired). Drift curves are fitted to the records following the procedure of Watts and Kontoyiannis (1990) and subsequently subtracted from each data point. While we estimate that the drift removed from the initial 60 days of each record could have residual errors of 0.5–1 mbar, the error remaining in the rest of each record is less than 0.15 mbar.

The pressure records were low-pass filtered using a 120-h cutoff frequency to remove ageostrophic signals. The resulting 23 pressure records were remarkably similar to one another on all time scales, with correlations between all pairs of records exceeding 0.93. This basin-wide signal, independent of location, is treated in relation to atmospheric forcing by Park and Watts (2005), but for calculating geostrophic deep currents it is dynamically unimportant. It is computed for each sampling period (1-h interval) as the mean of pressure records from three sites which have had the tidal signals removed. The basin-wide signal (shown later in upper left panel of Fig. 6) was subtracted from all 23 pressure records prior to leveling and mapping.

2.3. Leveling

The remaining subsections describe the procedures used to refer all pressure records to the same absolute geopotential, and the optimal interpolation method used to produce daily maps of the deep streamfunction. Except for modifications discussed here, the leveling and mapping procedures follow those presented in Watts et al. (2001).

Leveling was accomplished by assuming the measured mean deep currents were geostrophic to determine reference pressure differences between all sites. Optimal interpolation (OI) following the Gauss–Markov method of Bretherton et al. (1976) was used to map the deep streamfunction field from the 2-year mean current measurements.

Because the UB is enclosed along three sides by steep bathymetry, mapping of the mean flow field was improved by constraining the field so that no flow was allowed to go through these boundaries. This was accomplished by specifying the mean pressure to be a constant, $P_{bndy} = 0$, at 27 selected locations along the 300 m isobath (except along the eastern edge near Dok Island where the points followed the 800 m isobath). These boundaries were located about 10–30 km outside our mapping region. The streamfunction field obtained using just the mean measured currents and P_{bndy} was mapped to each PIES site ($\overline{P_{cm}}$). Next, the mean of each pressure record ($\overline{P}$) was determined over the same time interval as that used for the currents. The reference level for each PIES was calculated as $P_{ref} = \overline{P_{cm}} - \overline{P}$. Time series of leveled pressures were determined by adding these P_{ref} values to each respective pressure record.

2.4. Mapping

Daily maps of the deep pressure and current fields were obtained by combining leveled pressures and current measurements in a multivariate, nondivergent OI procedure. Once leveled, the pressure measurements alone could have been used to produce the maps. However, reduced errors result when both pressure and its gradients are supplied to the mapping procedure. Additionally, more realistic flow fields were obtained by preventing flow through the west, south, and east

boundaries of the UB, as had been done in the leveling procedure. Required inputs to the OI procedure are the correlation length r_0 and the noise-to-signal ratio E_0. The correlation length was determined empirically by least-squares fitting a Gaussian function to the spatial correlations estimated from pairs of leveled pressures. With the basin-wide mean removed, the correlation length of the leveled pressure records fell to 40 km. The value of E_0, estimated from the measurements, was set to 0.05 for both the pressure and current records.

Multiple mapping steps were used to produce the final daily maps. First, since the OI procedure operates with variables that have zero mean, a mean field was removed from the input data prior to the OI and restored to the output afterwards. Accordingly, the pressure field and its geostrophic velocity field were mapped both to the input locations and the output grid by a preliminary multivariate OI using the 2-year-long temporal means of the measured currents and leveled pressures and specifying $P_{bndy} = 0$. The means were then subtracted from the leveled pressure and current records to produce "demeaned" records. The no-flow through the boundary constraint only requires P_{bndy} to be a constant for each day; however, P_{bndy} may vary from day to day. To calculate the appropriate value for P_{bndy}, the OI procedure was applied to the demeaned current and pressure records without constraining the boundary to determine the daily streamfunction values at all 27 P_{bndy} sites and their average was calculated. Subsequently, the OI procedure was applied again to the demeaned pressure and current records including the daily mean P_{bndy} along the boundary. Gridded fields of the demeaned pressure and velocity were produced on a $1/8° \times 1/8°$ grid. The mean fields were restored to these fields to produce the final sequence of pressure and current maps.

3. Current observations

Stick plots of the currents exhibit a wide range in variability (Fig. 2) from weak and eddy-like to stronger and more persistent in speed and direc-

tion. Despite the range in variability, however, current speeds less than 2 cm/s dominate throughout the basin, accounting for 40–85% of the observed speeds at all but three sites.

Weak currents with variable direction are evident in many of the records shown in Fig. 2. For the most part, these sites are located in the interior of the UB away from strong topography. Lowest speeds are observed at sites M4-1 and EC2 (along the south border of the UB), where speeds less than 2 cm/s account for over 80% of the observations.

Relatively strong and steady currents are observed at four sites. Persistent and strong southward flow, sometimes exceeding 10 cm/s for a week and longer, are observed at M3-1 and EC4, sited close together along the Korean shelf. Stable currents of nearly equal strength, but directed towards the northwest and out of the UB, are observed at M1-2 (located over the KP). Few current reversals are recorded at any of these three locations. At EC1 (in the middle of the UIG), the flow is typically directed to the southwest, but several eddy reversals are observed.

Several high-velocity northward current events are observed at M2-1, but in general the current direction is more variable at that site. These events persist from as little as several days to many weeks.

Basic statistics for the low-passed filtered data are presented in Table 2 for the 2-year period and two 1-year-long subsets. Year 1 spans June 1999–June 2000 and Year 2 spans June 2000–June 2001. The mean current estimates could be biased low by the treatment of the stalls during processing. Alternate stall treatments were investigated at M2-1 and M1-5 where high percentages of stalls remained after processing. It was determined that the mean speeds at those sites could have been underestimated by approximately 8%. The standard error listed here is defined as the standard deviation divided by the square root of the number of degrees of freedom, which is estimated as the sample period divided by the integral time scale. The integral time scale is defined as the discrete integral of the time-lagged autocorrelation function from zero lag to the first zero crossing after demeaning and detrending the time series. This definition is the same as that employed by Chang

et al. (2002), allowing for direct comparison with their values; our Year 1 encompasses a similar time period to their 'common length' period. The integral time scales range from a minimum of 4 days at J1 to a maximum of 30 days at M1-2. For seven of the 13 sites with record lengths exceeding 660 days, the typical integral time scale exceeds 12 days; for the remaining six sites, typical values were roughly half that length.

We are motivated to examine the seasonal aspects of deep flow for several reasons: strong seasonal patterns had been observed in deep currents in the Japan Basin (Takematsu et al., 1999); the stratification throughout the thermocline exhibits a clear seasonal signal; and wind

forcing over the JES is monsoonal. Three-month-long seasonal averages of the u and v velocity components are presented in Fig. 3. Seasonally-averaged velocities generally range from 0 to 2 cm/s, except at M1-2, M3-1, and EC4 where they exceed 3 cm/s. Seasonal effects are clear only at EC4, where minimum southward velocities are observed in the fall period. At M2-1, evidence of a seasonal signal may be discernable from the maximum northward velocities in the Year-1 fall and Year-2 winter. No seasonal signal is evident at any other moorings.

On seasonal time scales, eddy kinetic energy (EKE) ranges from $0.2 \, \text{cm}^2/\text{s}^2$ at EC2 to $17.8 \, \text{cm}^2/\text{s}^2$ at M2-1, and mean kinetic energy
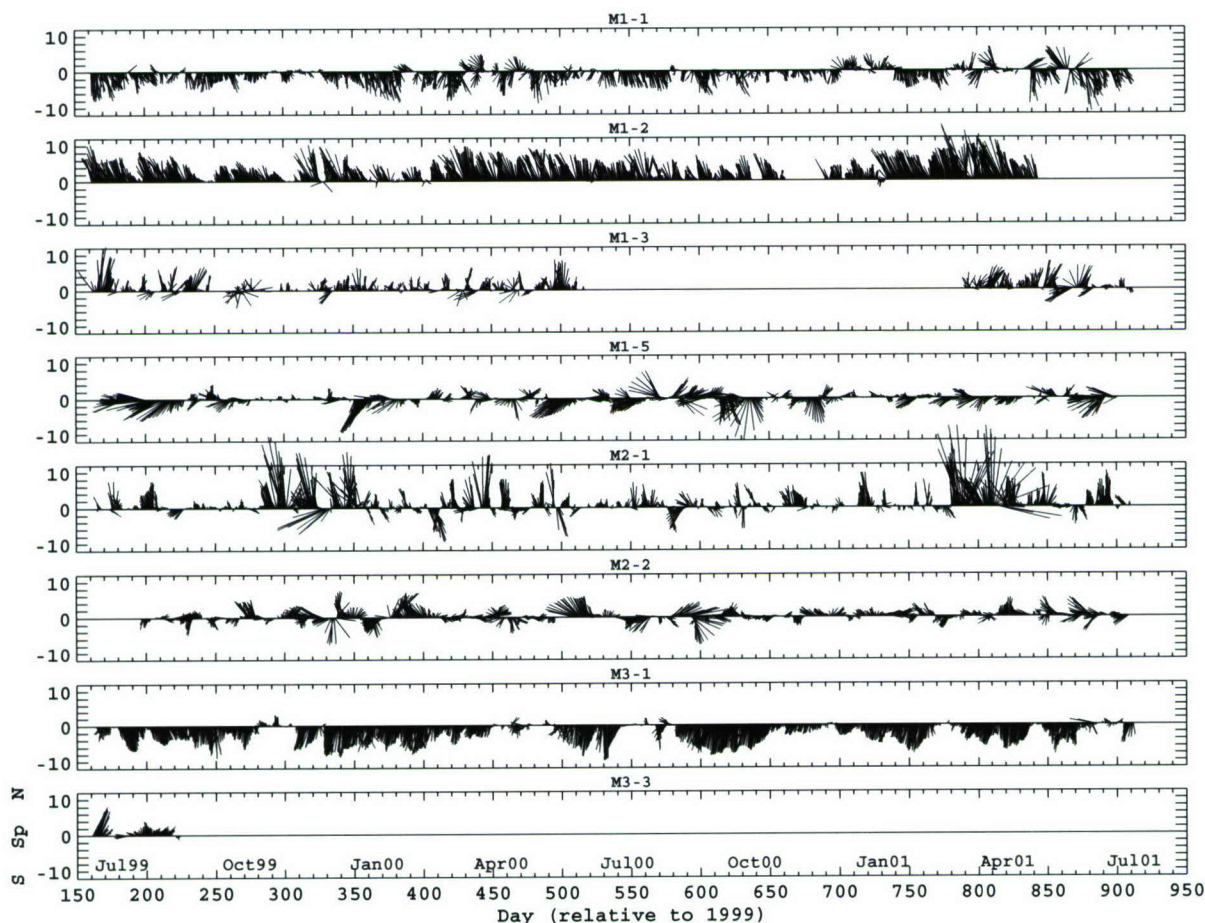

Fig. 2. Current stick diagrams (north is positive on the y axis) at 12-h intervals are shown. Tides and inertial currents have been removed using a low-pass filter with a 40-h cutoff frequency.
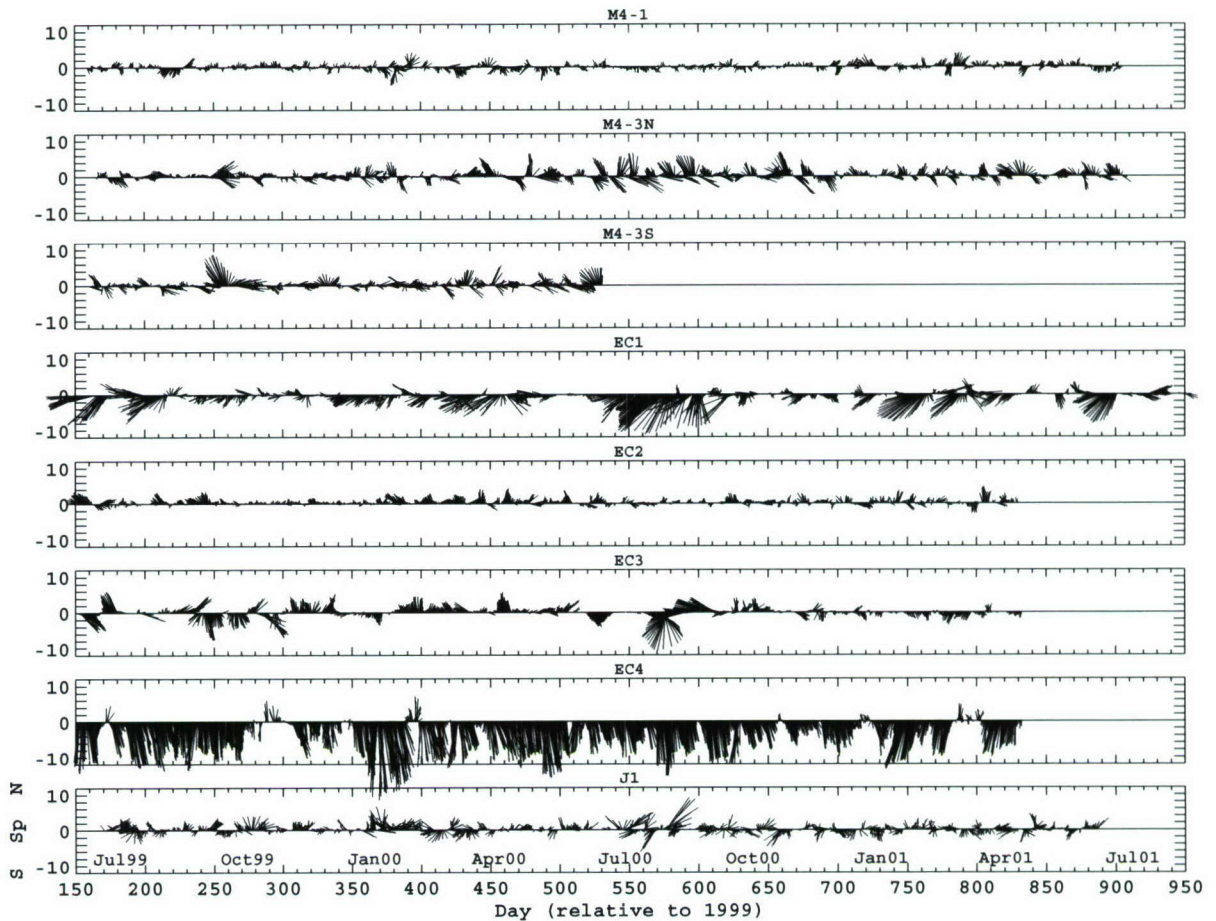
Fig. 2. (*Continued*)

Table 2
Basic statistics for the low-passed filtered data

Mooring	No. days time period	IT_u (day) IT_v (day)	$\overline{U}$ $\overline{V}$	σ_u σ_v	SE_u SE_v	U_{min} V_{min}	U_{max} V_{max}	$\overline{Spd}$ Spd_{max}	$\overline{Dir}$ Dir_{max}	EKE MKE
M1-1	747	9.50	0.09	1.40	0.16	−5.38	4.74	1.61	176.81	3.29
	Jun99–Jun01	9.07	−1.61	2.15	0.24	−9.50	5.72	9.71	167.06	1.30
M1-1	356	3.83	−0.01	1.23	0.13	−4.71	3.57	1.84	180.17	2.81
	Jun99–Jun00	8.51	−1.84	2.03	0.31	−7.41	4.08	7.80	156.44	1.70
M1-1	365	5.32	0.09	1.52	0.18	−5.38	4.74	1.29	175.90	3.64
	Jun00–Jun01	7.61	−1.29	2.23	0.32	−9.50	5.72	9.71	167.06	0.83
M1-2	661	12.84	−1.28	1.27	0.18	−8.19	3.98	3.81	340.38	3.36
	Jun99–Jun01	29.99	3.59	2.26	0.48	−2.52	13.22	14.30	337.56	7.25
M1-2	356	6.90	−1.34	1.24	0.17	−6.11	3.98	3.72	338.95	3.01
	Jun99–Jun00	17.58	3.47	2.12	0.47	−2.52	8.77	9.45	330.28	6.93
M1-2	305	5.30	−1.21	1.30	0.17	−8.19	3.04	3.91	341.96	3.74

Table 2 (*continued*)

Mooring	No. days time period	IT_u (day) IT_v (day)	$\overline{U}$ $\overline{V}$	σ_u σ_v	SE_u SE_v	U_{min} V_{min}	U_{max} V_{max}	$\overline{Spd}$ Spd_{max}	$\overline{Dir}$ Dir_{max}	EKE MKE
	Jun00–Jun01	24.96	3.72	2.40	0.69	−1.84	13.22	14.30	337.56	7.65
M1-3	480	4.11	−0.06	1.37	0.13	−6.01	6.01	1.16	357.09	2.71
	Jun99–Jun01	5.83	1.16	1.89	0.21	−4.24	10.53	10.68	9.66	0.68
M1-3	354	2.17	−0.07	1.12	0.09	−5.39	6.01	1.11	356.29	2.29
	Jun99–Jun00	5.28	1.11	1.83	0.22	−4.24	10.53	10.68	9.66	0.62
M1-5	737	13.73	−0.97	2.55	0.35	−11.70	9.24	1.09	243.37	4.89
	Jun99–Jun01	8.46	−0.49	1.82	0.19	−9.91	6.36	11.76	264.11	0.59
M1-5	353	13.35	−1.21	2.57	0.50	−11.70	4.48	1.29	249.16	4.85
	Jun99–Jun00	9.81	−0.46	1.76	0.29	−8.11	3.47	11.76	264.11	0.84
M1-5	365	6.04	−0.56	2.38	0.31	−8.43	9.24	0.73	230.54	4.51
	Jun00–Jun01	8.23	−0.46	1.84	0.28	−9.91	6.36	10.16	193.81	0.26
M2-1	746	5.15	−0.28	1.76	0.15	−12.12	15.63	1.54	349.48	7.30
	Jun99–Jun01	13.01	1.52	3.39	0.45	−8.02	19.02	19.16	352.71	1.19
M2-1	354	6.56	−0.44	1.77	0.24	−12.12	5.71	1.53	343.49	7.54
	Jun99–Jun00	7.22	1.47	3.45	0.49	−8.02	16.77	17.12	347.92	1.17
M2-1	365	5.11	−0.14	1.79	0.21	−6.98	15.63	1.53	354.76	7.35
	Jun00–Jun01	12.94	1.52	3.39	0.64	−6.08	19.02	19.16	352.71	1.16
M2-2	709	12.77	−0.31	2.30	0.31	−7.06	9.15	0.40	310.28	4.18
	Jun99–Jun01	8.31	0.26	1.76	0.19	−6.52	6.28	9.16	87.25	0.08
M2-2	317	10.66	−0.09	2.33	0.43	−7.06	6.65	0.37	345.68	4.69
	Jun99–Jun00	7.90	0.35	1.98	0.31	−6.38	6.28	8.50	47.85	0.07
M2-2	365	12.72	−0.39	2.25	0.42	−5.28	9.15	0.45	301.62	3.74
	Jun00–Jun01	7.75	0.24	1.55	0.23	−6.52	4.78	9.16	87.25	0.10
M3-1	748	12.67	−0.48	0.86	0.11	−6.17	3.91	2.70	190.26	2.65
	Jun99–Jun01	19.26	−2.66	2.13	0.34	−8.21	2.68	8.37	191.40	3.64
M3-1	354	11.55	−0.26	0.94	0.17	−4.95	3.91	2.61	185.78	2.67
	Jun99–Jun00	20.82	−2.60	2.11	0.51	−7.52	2.68	7.52	178.77	3.41
M3-1	365	5.14	−0.68	0.65	0.08	−3.51	1.62	2.95	193.43	2.44
	Jun00–Jun01	16.37	−2.87	2.11	0.45	−8.21	1.81	8.37	191.40	4.35
M3-3	59	11.31	0.16	1.46	0.64	−3.21	3.72	1.32	7.05	2.64
	Jun99–Jun00	7.86	1.31	1.77	0.64	−1.06	6.82	7.77	28.60	0.87
M4-1	748	4.51	0.24	0.95	0.07	−3.32	3.94	0.24	98.14	0.91
	Jun99–Jun01	4.75	−0.03	0.96	0.08	−4.29	3.42	4.46	196.10	0.03
M4-1	359	6.31	0.40	0.99	0.13	−3.32	3.94	0.42	106.18	1.00
	Jun99–Jun00	4.59	−0.12	1.01	0.11	−4.29	3.42	4.46	196.10	0.09
M4-1	365	4.05	0.09	0.90	0.09	−2.47	3.09	0.13	47.34	0.80
	Jun00–Jun01	4.33	0.09	0.89	0.10	−2.60	3.33	3.43	14.86	0.01
M4-3n	740	6.95	0.66	1.88	0.18	−5.03	6.73	0.76	59.59	2.96
	Jun99–Jun01	4.56	0.39	1.55	0.12	−4.30	5.70	6.98	124.58	0.29
M4-3n	352	9.89	0.68	1.76	0.30	−3.83	6.73	0.72	70.69	2.39
	Jun99–Jun00	4.90	0.24	1.30	0.15	−3.97	5.43	6.87	101.40	0.26

Table 2 (*continued*)

Mooring	No. days time period	IT_u (day) IT_v (day)	$\overline{U}$ $\overline{V}$	σ_u σ_v	SE_u SE_v	U_{min} V_{min}	U_{max} V_{max}	$\overline{Spd}$ Spd_{max}	$\overline{Dir}$ Dir_{max}	EKE MKE
M4-3n	365	5.83	0.65	2.00	0.25	−5.03	5.97	0.82	51.99	3.52
	Jun00–Jun01	4.42	0.50	1.74	0.19	−4.30	5.70	6.98	124.58	0.34
M4-3s	358	5.28	1.10	1.95	0.24	−4.18	8.63	1.12	80.20	2.71
	Jun99–Jun00	4.74	0.19	1.28	0.15	−3.23	7.31	8.63	89.81	0.63
EC1	777	9.25	−1.55	2.69	0.29	−10.32	8.54	1.87	235.78	5.59
	Jun99–Jun01	10.73	−1.05	1.99	0.23	−9.42	3.70	12.23	225.69	1.75
EC1	354	7.73	−1.82	2.43	0.36	−10.32	5.74	2.04	243.56	4.13
	Jun99–Jun00	7.27	−0.91	1.54	0.22	−6.97	3.04	10.44	228.27	2.07
EC1	356	8.65	−1.51	2.80	0.44	−9.66	8.54	1.96	230.38	6.66
	Jun00–Jun01	9.65	−1.25	2.34	0.39	−9.42	3.70	12.23	225.69	1.92
EC2	670	7.09	0.20	1.01	0.10	−3.10	3.92	0.50	24.24	0.89
	Jun99–Jun01	4.59	0.45	0.87	0.07	−2.53	3.84	4.24	67.71	0.12
EC2	359	7.50	0.08	1.08	0.16	−3.10	3.92	0.64	7.16	0.92
	Jun99–Jun00	4.51	0.64	0.82	0.09	−1.62	3.52	4.24	67.71	0.21
EC2	311	5.97	0.35	0.91	0.13	−2.86	3.57	0.42	55.47	0.78
	Jun00–Jun01	4.08	0.24	0.86	0.10	−2.53	3.84	3.84	358.14	0.09
EC3	669	20.18	0.04	2.11	0.37	−7.35	6.77	0.14	160.54	4.09
	Jun99–Jun01	14.83	−0.13	1.93	0.29	−9.14	5.03	9.42	195.26	0.01
EC3	355	10.66	0.50	1.67	0.29	−3.43	6.77	0.57	61.28	3.53
	Jun99–Jun00	11.09	0.27	2.06	0.36	−6.45	5.03	8.51	127.30	0.16
EC3	315	23.31	−0.47	2.41	0.66	−7.35	5.09	0.74	218.90	4.29
	Jun00–Jun01	15.93	−0.58	1.66	0.37	−9.14	3.48	9.42	195.26	0.28
EC4	673	15.06	0.52	1.09	0.16	−4.58	4.14	5.30	174.32	7.45
	Jun99–Jun01	12.01	−5.27	3.70	0.49	−18.53	6.09	18.54	181.89	14.03
EC4	359	6.87	0.77	1.07	0.15	−2.34	4.14	6.10	172.75	8.65
	Jun99–Jun00	12.68	−6.05	4.02	0.76	−18.53	6.09	18.54	181.89	18.62
EC4	314	10.29	0.24	1.05	0.19	−4.58	2.40	4.38	176.82	5.26
	Jun00–Jun01	8.74	−4.38	3.07	0.51	−12.93	4.14	12.93	181.29	9.61
J1	705	3.80	0.00	1.68	0.12	−5.10	8.13	0.27	1.00	2.30
	Jun99–Jun01	5.06	0.27	1.34	0.11	−5.17	7.70	10.23	48.89	0.04
J1	347	3.51	−0.00	1.60	0.16	−5.10	5.67	0.51	359.91	2.08
	Jun99–Jun00	6.57	0.51	1.26	0.17	−3.17	5.60	6.01	70.30	0.13
J1	354	4.07	−0.00	1.75	0.19	−4.73	8.13	0.03	357.88	2.46
	Jun00–Jun01	4.56	0.03	1.37	0.16	−5.17	7.70	10.23	48.89	0.00

Integral time scales for each current component (IT_u and IT_v), average current components ($\overline{U}$ and $\overline{V}$, where U is positive eastward and V is positive northward) standard deviations (σ_u and σ_v), standard errors in velocity, (SE_u and SE_v), velocity minima (U_{min} and V_{min}), velocity maxima (U_{max} and V_{max}), average speeds ($\overline{Spd}$), average directions ($\overline{Dir}$, measured clockwise where $0°$ is North), maximum speed (Spd_{max}) directions of the maximum speeds (Dir_{max}), eddy kinetic energies (EKE) and mean kinetic energies (MKE) are presented for the 2-year period and individual years. Units are cgs.
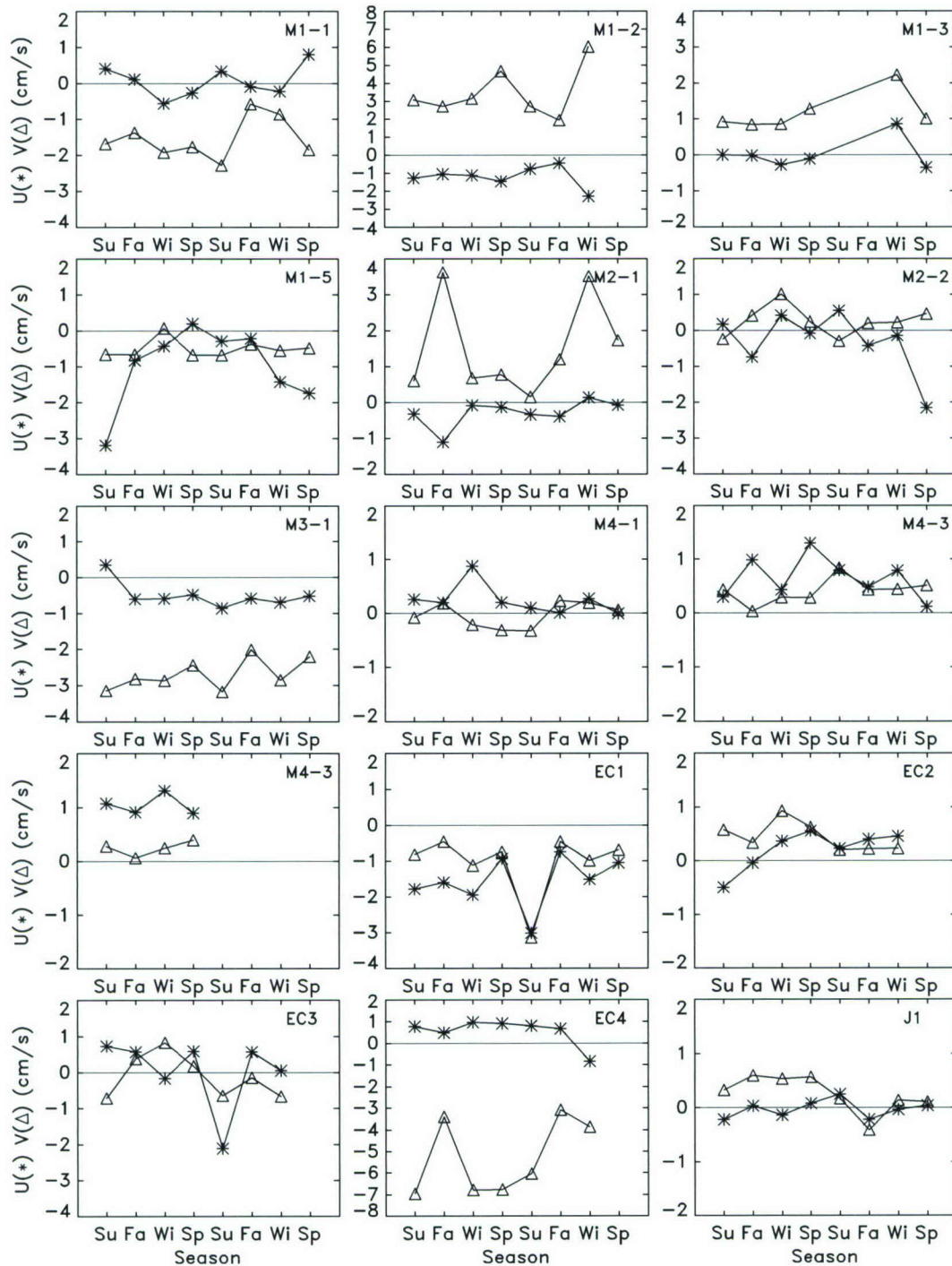
Fig. 3. Average east–west (U, *) and north–south (V, $\triangle$) velocity components are shown for Summer (Su: July, August, September), Fall (Fa: October, November, December), Winter (Wi: January, February, March), and Spring (Sp: April, May, June).

(MKE) ranges from near zero at many of the moorings to over $24 \, cm^2/s^2$ at EC4 (Fig. 4). MKE is larger than EKE at M1-2, M3-1, and EC4, locations where the mean currents are best determined. EKE clearly dominates at the other moorings because of weak mean flows. There are no clear seasonal signals in either EKE or MKE, and their patterns are quite different between moorings.

The averaged vectors for Year 1 and Year 2 and the 2-year averages can be compared in Fig. 5. The flow directions of the mean currents are very similar from year to year, except where mean currents are so weak at M4-1 and EC3. At sites around the edges of the UB, the mean vectors follow the bathymetry closely. The southward flows at M1-1, EC1 and M1-5 indicate that strong deep inflow into the Ulleung Basin occurs across the Korea Plateau (near the shelfbreak in latitudes 37–38°N) as well as through the UIG. Northward mean flows are observed on the eastern portion of the KP near Ulleung Island.

Mean velocities decrease by approximately 0.5–1 cm/s from Year 1 to Year 2 at M1-1, M1-5, EC2, and J1. At site EC4, the velocities decrease by about 2 cm/s during the second year. These differences are minor, and the annual mean currents are quite stable in both speed and direction.

4. Pressure observations

The 2-year-long records of leveled pressures are presented in Fig. 6. With the basin-wide signal (uppermost left panel) removed from the records, the residual signal in the leveled pressures is weak. Seven of the 23 records exhibit peak-to-peak fluctuations of less than 3 mbar and an additional eight have ranges under 4 mbar. The maximum range observed is about 10 mbar, at site P1-4.

The largest standard deviations (std > 1 mbar in Fig. 6) occur at sites P1-4, P2-1 and P2-5. At P1-4, the fluctuations are short bursts of intensified pressure lows. Since this site is located along the edge of a deep, narrow channel northeast of Ulleung Island (Fig. 1), these fluctuations may be associated with pulses of stronger current flowing through the channel. In contrast at P2-5, longer period (> 400 days) pressure fluctuations dominate. At site P2-1, the high variability is consistent with the high EKE observed at the neighboring M2-1 current mooring.

5. Deep flow patterns

From current measurements at four locations in the UB, Chang et al. (2002) reported deep mean flow that is consistent with cyclonic circulation. However, the paucity of instrumented sites in that experiment left much of the UB unsampled. Here, we combine their observations with our more extensive array of RCMs and PIESs to examine the deep flow patterns throughout the UB. In addition to increased areal coverage, this highly instrumented array has the advantage of better spatial resolution by combining data from PIES sites on an approximate grid spaced 50–60 km and the RCMs sited near the middle of the squares.

The mean currents and standard deviation ellipses for the 2-year period, Years 1 and 2, and quarter years are displayed together with the corresponding dynamic pressure maps in Fig. 7. The pressure maps (Fig. 7a) are fields of perturbation pressure relative to a deep reference hydrostatic pressure (whose actual value is immaterial). Below 1000 m the dynamic pressure is nearly depth-independent, because the vertical shear is almost negligible below the pycnocline. The deep current measurements used for leveling the pressures geostrophically therefore could all be treated as reference velocities at the reference pressure (even though the RCM sites ranged in depths from 1200–2300 m). We estimate that departures from geostrophic and hydrostatic (thermal wind) balance in this deep circulation (such as causing small cross-isobath components of flow) are less than 0.1 mbar, and therefore have negligible effects on the mapped fields presented.

Currents at sites that have means larger than their respective ellipses are relatively stable (Fig. 7b). In this sense, the stable annual currents are confined to two sites along the Korean shelf and one site over the Korea Plateau. At the other sites, the mean current vector is located entirely
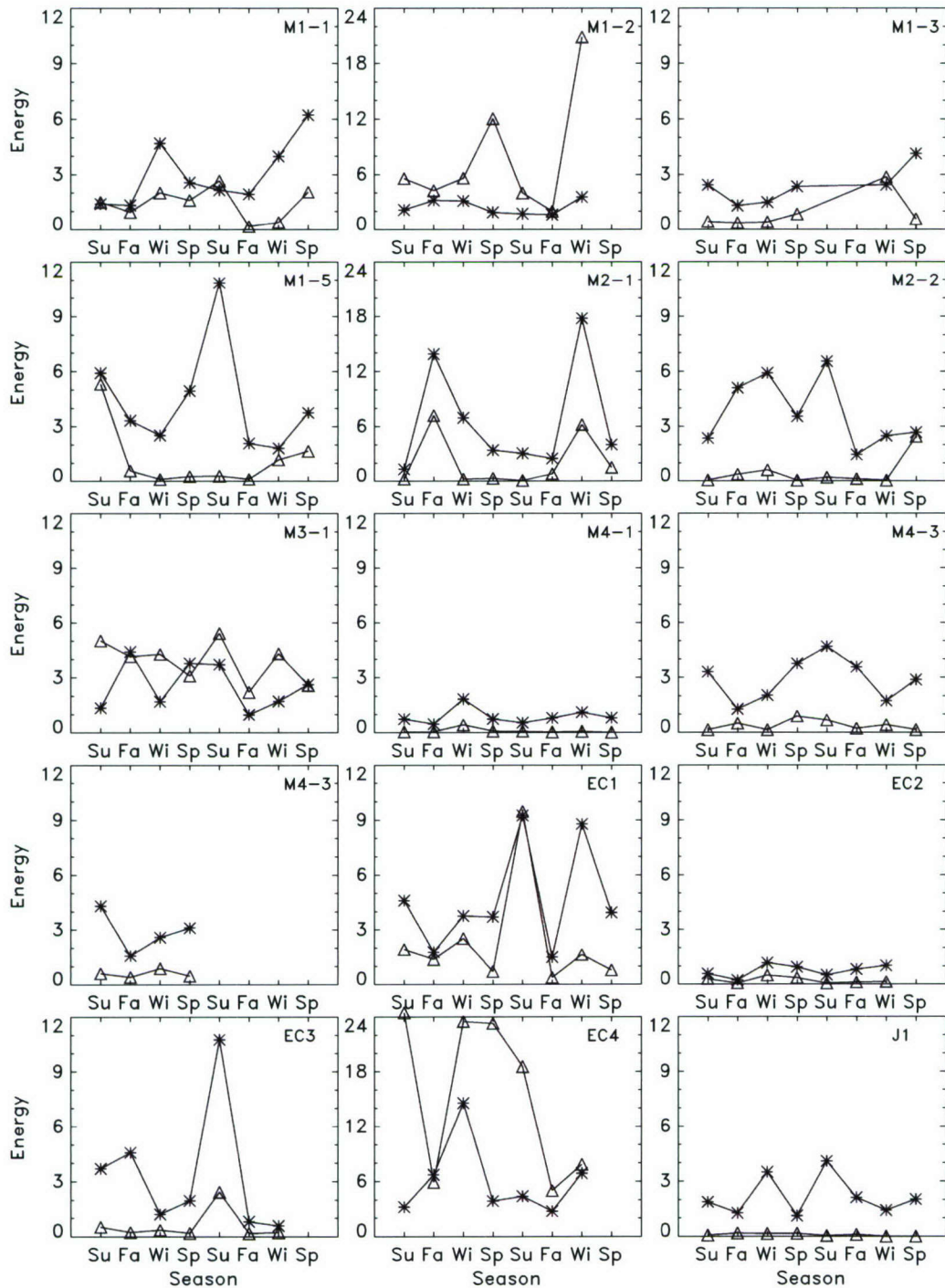
Fig. 4. Average eddy kinetic energy, EKE (*) and mean kinetic energy, MKE (△) in units of cm^2/s^2 for seasons described in Fig. 3.
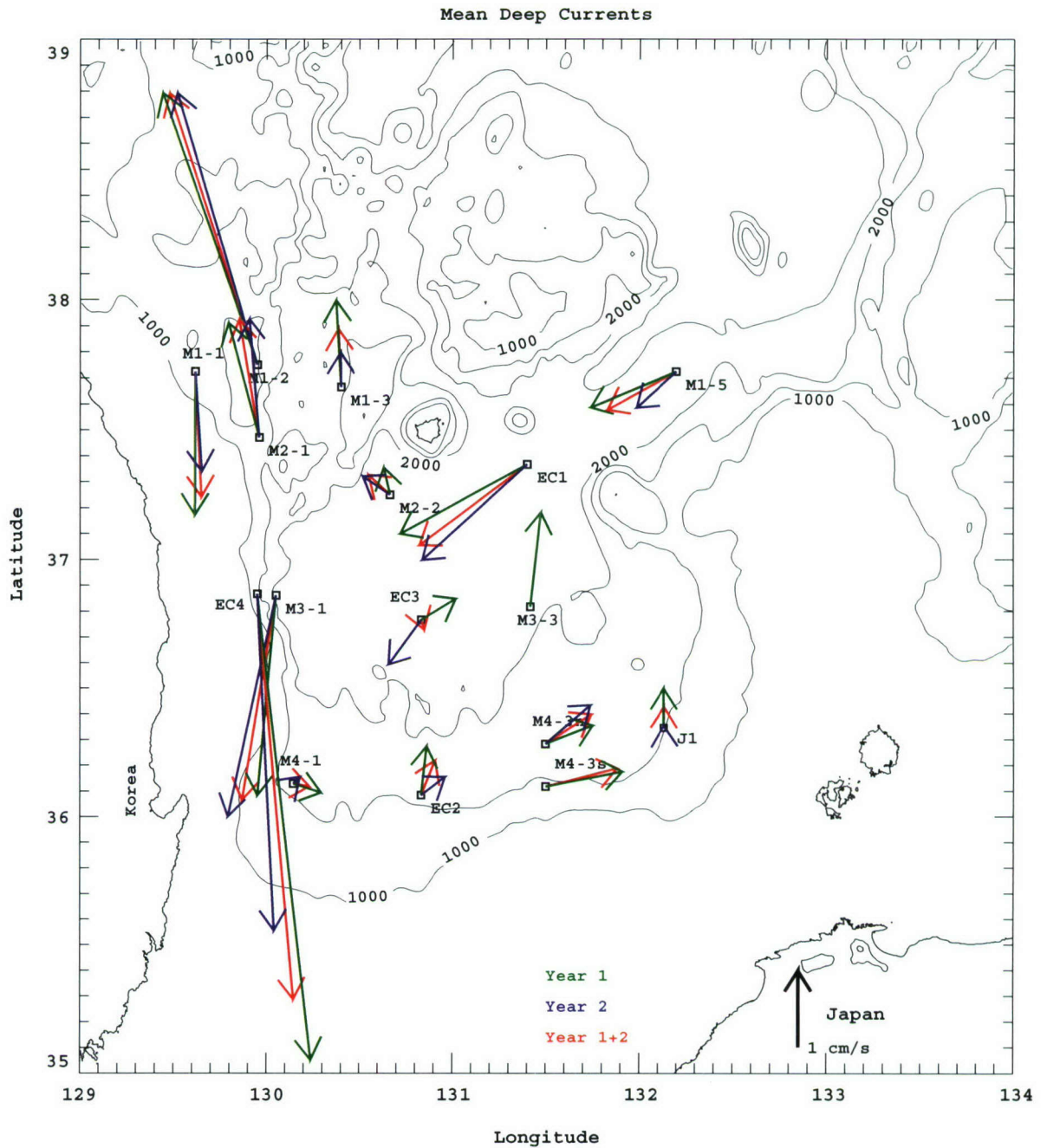
Fig. 5. Deep currents averaged over each year and over both years (June 1999 to June 2001). Bathymetry (Choi, 1999) units are meters.

within an almost circular ellipse, which indicates no prevalent current direction for daily currents. However, almost all of the mean currents (except for M2-2, M4-1, EC3, and J1) are significant for annual time scales using the criteria that the standard error (6–12 times smaller than the
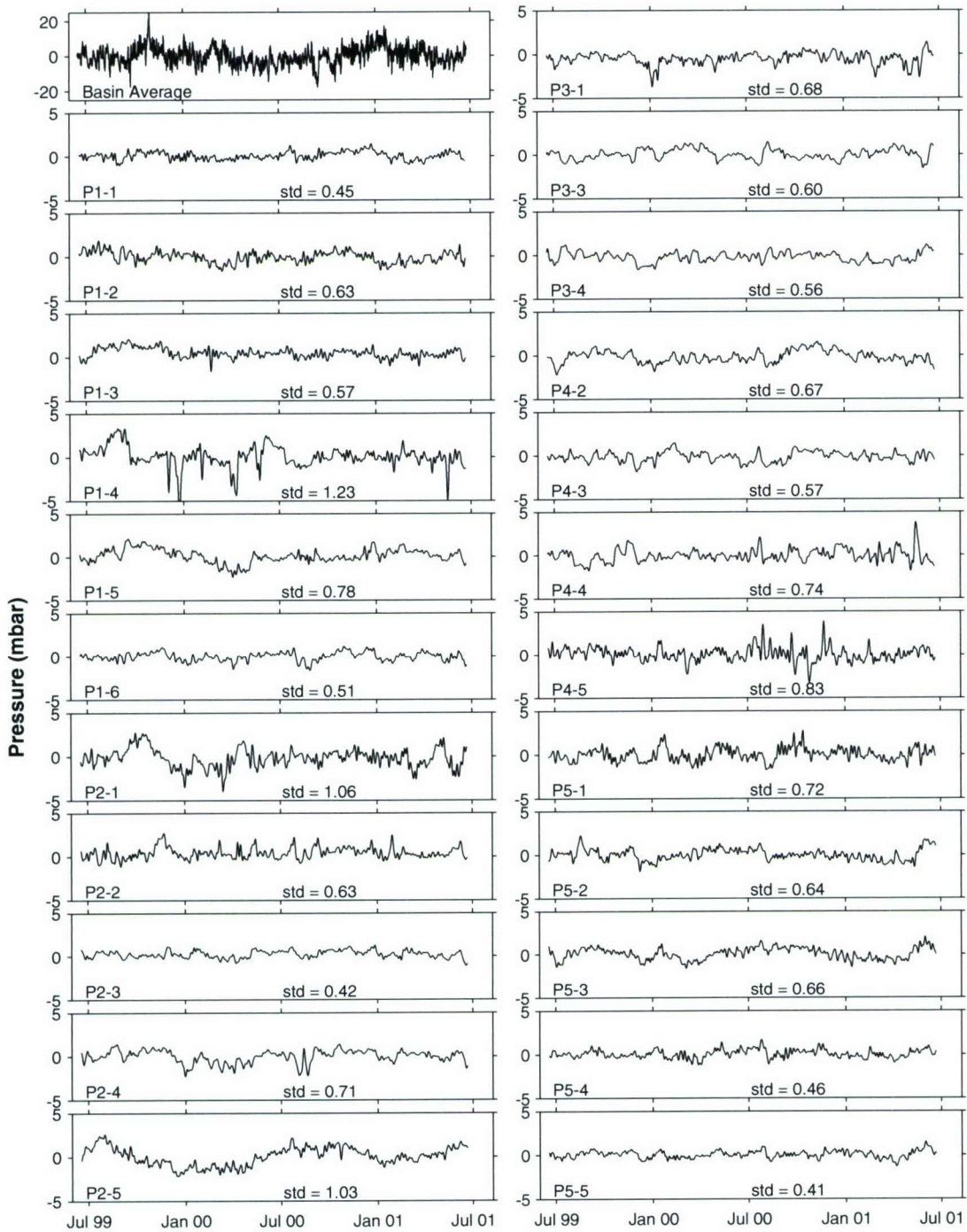
Fig. 6. Time series of leveled pressure at 23 PIES sites and the basin-wide pressure signal removed from each record prior to leveling. The records at the individual sites have been low-pass filtered using a 5-d cutoff period and are plotted at 12-h intervals. The basin-wide signal has not been low-pass filtered and is shown at hourly intervals. Standard deviations are in millibars.

Fig. 7. Dynamic pressure fields (A) corresponding to the mean currents with their standard deviation ellipses (B). Two-year and individual-year averages (left column), Year 1 quarterly means (middle column), Year 2 quarterly means (right column). Geostrophic current vectors are shown for every other grid point on the pressure fields. Contour interval is 0.25 mbar. The velocity scale in the lower right corner of each panel indicates 2 cm/s.

Fig. 7. (*Continued*)

standard deviation, as listed in Table 2) is smaller than the larger current component.

The 2-year and each 1-year averaged flow fields are all remarkably similar, corroborating that the means are stable. As was suggested by the mean vectors in Fig. 5, a mean cyclonic circulation pattern in the UB is evident in these maps. However, the higher resolution afforded by these dynamic pressure fields reveals that the deep circulation consists of at least two cyclonic cells. The cells range in size from about 50 to 100 km, although the two-cell pattern is barely resolved by the geographical spacing of our measurement sites. Low-pressure cells are found along the shelf break off Korea and in the interior of the UB. The low along the shelf break is usually more intense than the low in the eastern half of the UB. These cells are separated by a high-pressure ridge extending southward from the vicinity of Ulleung Island. In addition to the low-pressure cells, the mean deep flow field is characterized by a pressure high around Ulleung Island, which extends to the north.

The stability of the mean circulation over the 1- and 2-year periods lead us to examine the means over shorter time scales. Quarterly (3-month-long) means were determined for both Year 1 and Year 2 (Fig. 7). These quarterly-mean dynamic pressure maps exhibit a wide variety of features, with some features common to all periods and others distinct. For all quarterly periods, southward flow is found along the Korea shelf break, while northward flow is found over the KP farther offshore. The intensity of these features varies between averaging periods. For example, the low-pressure cell off the shelf was both spatially extensive and strong during January–March 2000, whereas it was small and weak during October–December 2000. The current ellipses are noticeably smaller during this latter period. Similar variations in intensity and size are apparent for the anticyclonic cell near Ulleung Island. At times the anticyclone penetrates deep into the interior of the UB (January–March 2000) while at others it is confined farther north (July–September 1999). Despite these differences, the current at M1-2, located between the high- and low-pressure cells over the KP, is remarkably strong and steady during nearly all quarterly periods. The exception is October–December 2000, when the low-pressure cell is weak and the high extends over the whole KP.

The circulation in the southeastern region of the UB near the Oki Spur is weak and variable. The quarterly means exhibit both cyclonic and anticyclonic circulation patterns with features of short spatial scale. Differences in the orientation of the standard deviation ellipses for Year 1 at two current meters along the southern boundary, separated by only 18 km, highlight the low coherence and shortness of scales.

The mapped fields indicate regions of deep flow into and out of the UB. Transport into the basin occurs in two locations, along the shelf break off Korea and through the UIG. The mapped fields and current vectors show that transport out of the UB takes place over the KP. Northward flow across the plateau is associated with an anticyclonic circulation pattern that extends around Ulleung Island. However, because the KP is about 500 m shallower than the UB, the deeper waters in the basin would either be blocked or any component of flow normal to the ridge would imply substantial vertical motion over the rise. The dynamic-pressure maps also suggest that flow exits the UB on the southeastern side of the UIG past the northern tip of the Oki Spur. The annual mean and many of the quarterly-mean maps indicate outflow past Dok Island associated with a low-pressure anomaly in the vicinity of the UIG channel. Furthermore, flow out of the region is associated with a high-pressure cell in the northeast corner of the mapped fields. Unfortunately, there are no directly measured currents in either area to confirm these findings.

6. Modelled currents

The NRL Layered Ocean Model (NLOM) is used here to simulate the abyssal circulation in the JES to further examine deep flow patterns observed by the measurements. NLOM is a semi-implicit primitive equation ocean model with vertically integrated model equations for each layer. The fundamental model design is described in detail in Hurlburt and Thompson (1980),

Table 3
NLOM model parameters

Grid resolution	$1/32°$ (lat) $\times 45/1024°$ (lon)
Number of vertical layers	4
Layer interfaces	60 m, 130 m, 250 m
Wind stress forcing	Hellerman and Rosenstein (1983)
KTS inflow	Mean transport of 2.0 Sv plus seasonal signal
Outflow	Tsugaru and Soya straits balancing KTS inflow

although Wallcraft (1991) has significantly enhanced the current version. The dynamics of the circulation, including the coupling of the abyssal and surface circulations, and the impact of bottom topography is described in Hogan and Hurlburt (2000). That work also includes a complete description of the JES model configuration used here. A summary of the pertinent model parameters is given in Table 3.

NLOM depicts several distinct circulation patterns in the UB. Snapshots of the NLOM abyssal circulation show that the cyclonic pattern may consist of a single large cyclonic cell encompassing almost the entire UB (Fig. 8a) or may be composed of multiple smaller cells, both cyclonic and anticyclonic (Fig. 8b). Like the observed fields, the NLOM flow patterns are highly variable in both space and time. In general these patterns resemble those actually observed with the PIES and RCM measurements (Fig. 7). Yet the single cyclonic pattern that is commonly produced by NLOM is observed less often. However, since the simulated currents are forced with monthly climatology and do not assimilate oceanic data, they have no correspondence with the actual date of the observations. Hogan and Hurlburt (2000) found that the deep flows in the Ulleung Basin are driven by mesoscale flow instabilities rather than surface wind forcing.

Annual mean NLOM current vectors with standard deviation ellipses are determined at locations near the current meter positions (Fig. 9). The NLOM locations are shifted slightly from the actual mooring locations in order for the model bathymetry to more closely match actual depths at the measurement sites. Overall, the agreement between measured annual current

means and ellipses (Fig. 7b) and those produced from NLOM is reasonable. Similar to the measurements, the NLOM vectors show inflow into the UB through the UIG and over the KP. They also show flow exiting the basin over the KP near Ulleung Island. Yet, some differences exist. For example, the NLOM values tend to be smaller than the measurements. This underestimation may be an artifact of the model because its abyssal current represents a thick bottom layer below 250 m.

Nevertheless, because the modelled abyssal currents compare favorably with the measured currents they are used to help examine finer details of the circulation pattern at a few selected locations. Three additional "simulated moorings" are included in Fig. 9. MM1 and MM3 are placed in the southeastern portion of the UIG to examine the flow on the side of the channel where no current measurements were made. The NLOM mean currents at both locations are northeastward, supporting the pathway for deep flow out of the UB suggested in some maps by the observations (Fig. 7). This northeastern outflow is clearly evident in both NLOM snapshots shown in Fig. 8. MM2 is placed on the western side of the interior of the UB to examine the flow regime between the two cyclonic cells revealed by the moored array. The modelled currents at this simulated mooring suggest a connection between the two circulation cells.

The NLOM currents can be used to calculate volume transport along a section between Ulleung Island and Dok Island, spanning approximately between the 1000 m isobaths. Transport below 250 m into the UB on the northwestern end of the section in the deep layer of NLOM (250 m to the bottom) is 0.68 Sv (1 Sv is $10^6 \text{ m}^3/\text{s}$). Transport out of the basin on the southeastern side is 0.38 Sv, yielding a net transport of 0.3 Sv into the basin. If the net inflow into the UB is upwelled, the residence time in the basin can be approximated dividing the volume of the basin by the net transport. Then for a depth of 1700 m and an area approximated by 200 km square, the residence time for the abyssal waters is about 7 years. The associated upwelling rate, estimated by transport divided by area, is about 60 cm/day.

7. Discussion

There is a marked lack of horizontal coherence in most of the deep flows. The dissimilarities are apparent in the stick vector plots of the low-passed currents shown in Fig. 2. For example, little coherence is evident in the close neighbor records from sites M4-3N and M4-3S, located along the
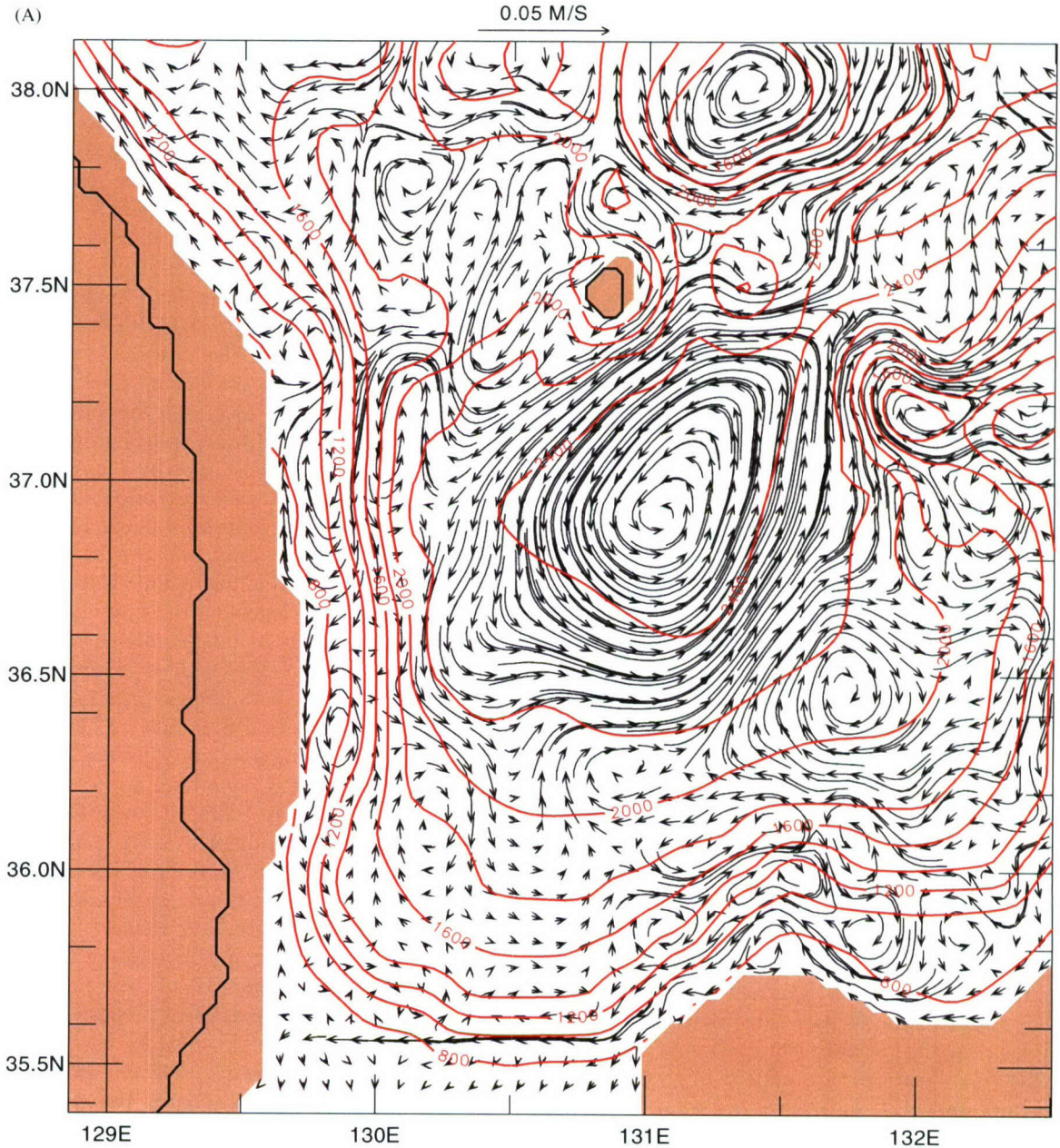

Fig. 8. Currents in the abyssal layer (arrows) from NLOM and bottom topography (red contours) are shown for two snapshots consisting of one large cyclonic cell in (A) and multiple cells in (B).
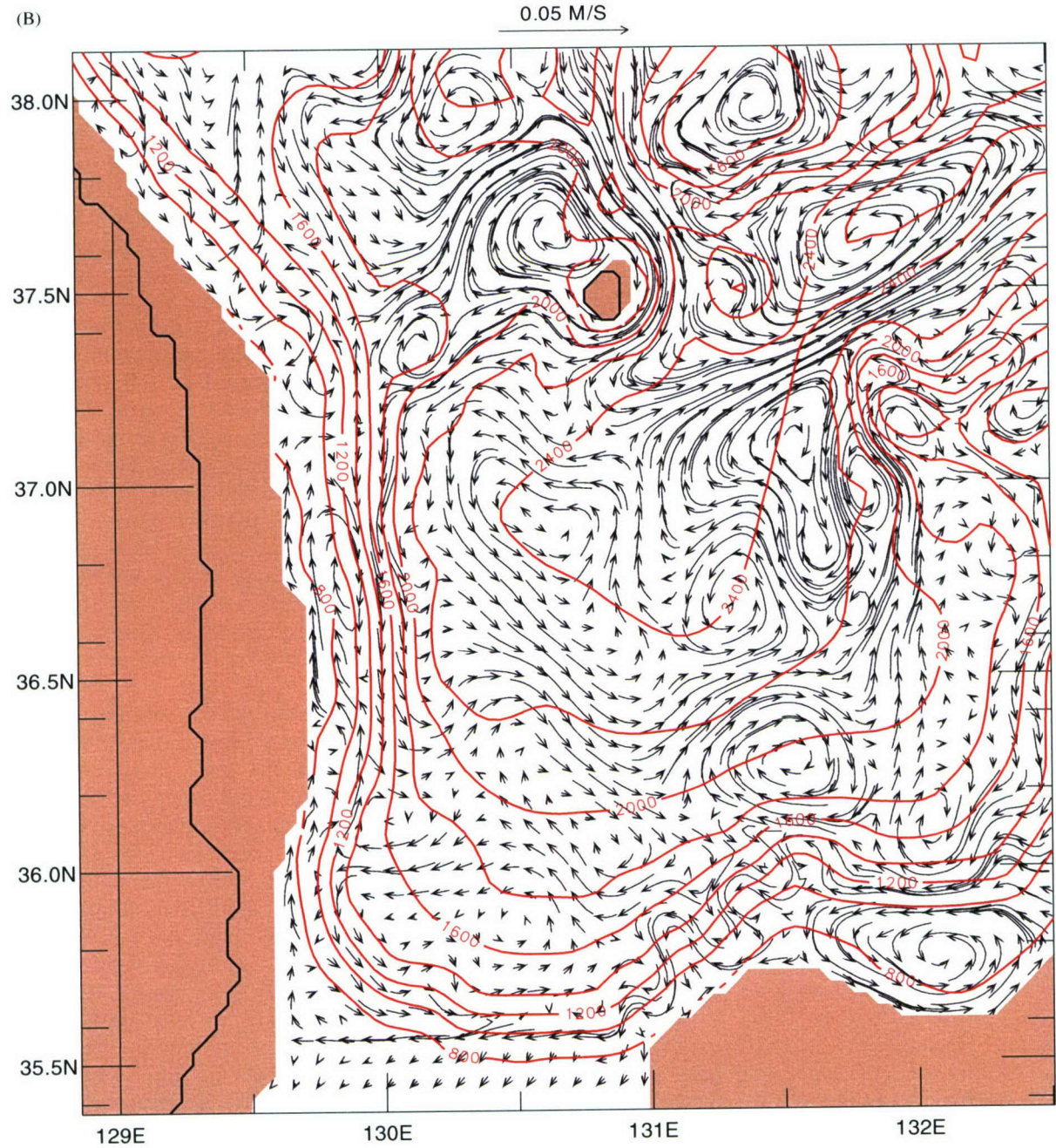
Fig. 8. (*Continued*)

southern edge of the UB (separated by less than 20 km). Eddy-like variability is observed in most of the records, especially at sites in the interior of the

UB. Strong eddy events with speeds exceeding 10 cm/s are observed at some of these sites, while at others the currents never reach 4 cm/s. In
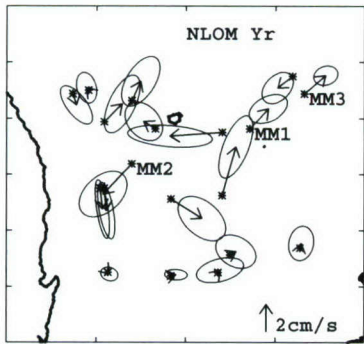
Fig. 9. NLOM mean currents and their corresponding standard deviation ellipses are shown for a 1-year period. Note that three additional simulated moorings (MM1, MM2, and MM3) have been added.

contrast, the currents at four sites exhibit relatively steady speed and direction when compared to the eddy variability. Three of these sites are located along the steep topography off Korea. Topographic steering accounts for the elongated variance ellipses at these sites.

Better correlations are found in the deep flows on the steep shelf break off Korea. Persistent southward flows are observed at EC4 and M3-1, which are located within about 10 km of each other. The instrument depths differ by nearly 950 m, and the average flow decreases from about 5 cm/s at the shallower site to 3 cm/s at the deeper site. Stronger currents occur in bursts over a period of a month or two, interspersed with weak currents. Such a current pattern is suggestive of a meandering deep western boundary current. There are few current reversals at either of these two locations. One of these reversals occurs in both records in late October 1999. At that time, transport through the Korea/Tsushima Strait reached a maximum (Teague et al., 2002) and the upper layer of the entire UB warmed considerably (Mitchell et al., 2005). This suggests that the strengths of the upper and lower circulations may be coupled.

The Korea Plateau is a confluence region for the currents in the surface layer, where the northward-flowing East Korean Warm Current (EKWC) meets the southward-flowing North Korea Cold Current (NKCC). They join to form the Subpolar

Front (also called the Polar Front), which separates from the coast and flows towards the east-northeast (Preller and Hogan, 1998) along the northern edge of the UB. Located beneath this surface confluence were several deep RCMs and PIESs that measured flows both into and out of the UB. Fairly steady southward flow, averaging 1.6 cm/s, is observed at the mooring closest to the Korean shelf. This is consistent with earlier current observations of Lie et al. (1989) at a similar location. Unexpectedly, however, the two moorings located only about 30 km farther offshore observe flows of equal or greater strength in the opposite direction. Northward flow is also observed at a third site on the KP closer to Ulleung Island. Surprisingly, the most intense northward flow is observed at the northernmost of the three moorings (site M1-2) at a site separated from the steepest topography. The dynamic pressure maps (Fig. 7a) show cyclonic circulation near the Korean shelf adjacent to an anticyclonic circulation around Ulleung Island. Mooring M1-2 is nearly always situated in the relatively high-gradient region between these two circulation cells where stronger flows should occur.

Topographic effects on the currents are clearly evident in the southwesternmost corner of the UB near the KTS. Here the shelf break changes orientation from north/south along the Korean coast to east/west along the southern boundary. Simultaneously, the topography also changes abruptly from steeply-sloped to more gradual. Neighboring moorings along the steep shelf exhibited strong southerly flows and a continuation of such flow might be expected at the mooring in the southwestern corner (M4-1) as well. Instead, the currents are weak and directed east-south-easterly similar to the orientation of the local bathymetry. Since the isobaths are also spaced nearly ten times farther apart, it is reasonable for isobath-following mean currents to spread out, in which case their corresponding speed would decrease by an order of magnitude.

Chang et al. (2002) find direct evidence of southwestward inflow, averaging about 2 cm/s, through the UIG using a single mooring. Such a current for an effective channel width of 50 km and a thickness of 2000 m yields a transport of 2 Sv.

This inflow must be balanced by a combination of outflow and upward mass flux into the thermocline. In this experiment, deep flow was measured along the channel as far east as the tip of the Oki Spur with a set of five PIESs and two RCMs. The averaged pressure fields show a low-pressure anomaly covering this region, with currents flowing towards southwest along the northwestern flank of the anomaly. A small region of higher pressure occurs east of Dok Island and along the Oki Spur. This pattern suggests that the deep flow may exit out of the UB along the eastern edge of the UIG. NLOM model results also indicate flow leaving the basin in this region. However, the short spatial scales and the lack of direct current observations in the UIG region prevent confirmation that the flow reverses.

Evidence of deep outflow from the UB is observed on the Korea Plateau, where we had eight relatively closely spaced instruments. It appears likely that most of the deep UIG inflow exits again to the north in the sub-thermocline. Deep outflow should dominate over upwelling, by the following argument: If there were uniform deep inflow across the UIG channel, the transport would be about 2 Sv; and if there were no compensating deep outflow, the residence time would be very short, only 1 year in the deep UB; the upper waters would then be a mixture of nearly equal amounts of warm inflow from Tsushima Strait and upwelled near-zero °C deep water. As a counterexample, the upper Ulleung Warm Eddy can persist for many months with properties similar to the inflowing KTS waters, indicating
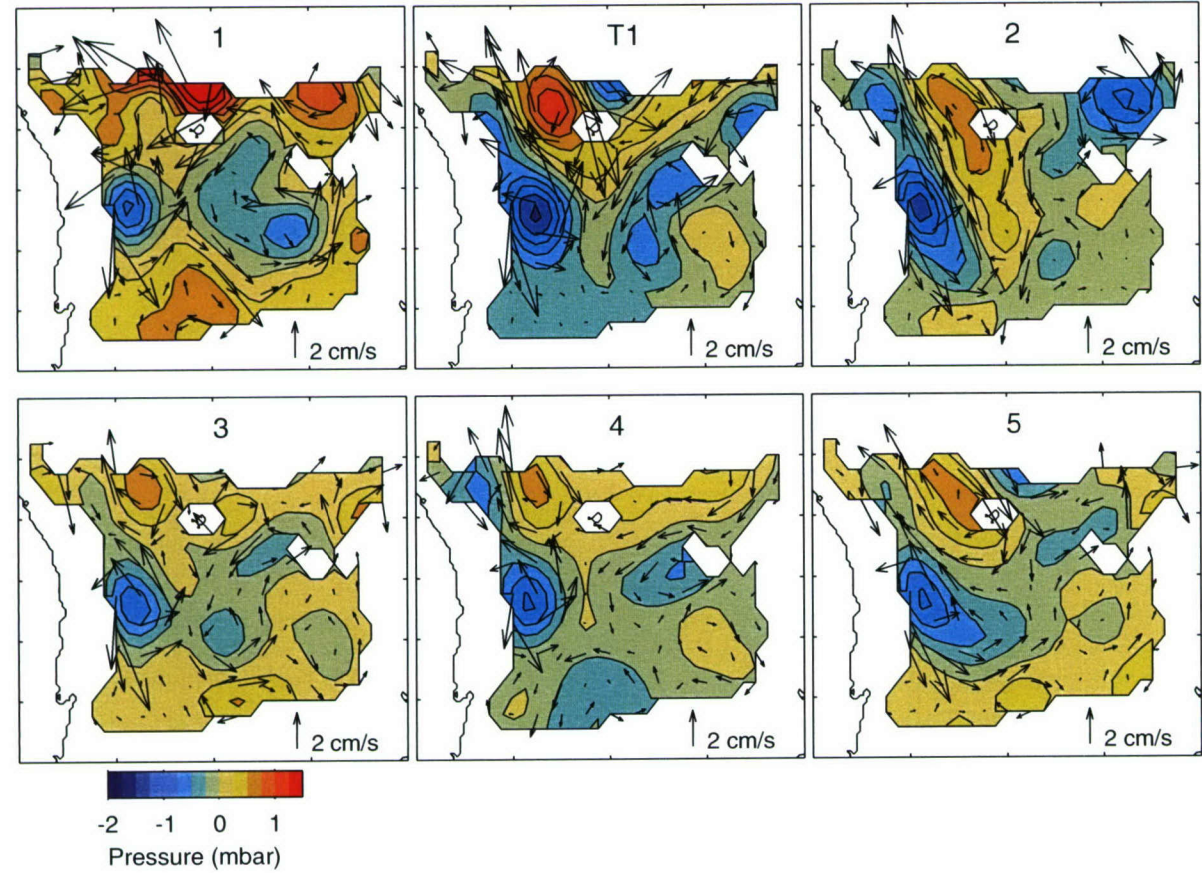

Fig. 10. Dynamic pressure fields averaged for the same time periods as those for temperature at 100 dbar shown in Fig. 3 of Mitchell et al. (2005).

weak upwelling. Consequently it seems likely that the deep inflows and outflows nearly compensate one another.

While Takematsu et al. (1999) found a significant seasonal pattern at deep moorings in the Japan Basin, seasonal variability is weak or absent at all of our moorings in the UB. Weak seasonality implies that the deep currents are not directly forced by surface winds nor by local strong changes in upper-layer stratification due to inflow from the Tsushima Current, nor by remote wintertime convection. However, since qualitative differences do exist between the quarterly-mean pressure fields, it is interesting to explore other possible correlations with the upper-layer variability. Mitchell et al. (2005) use the PIES acoustic time measurements to examine the temperature field at 100 dbar. They find five to six distinct regimes that persist for 45 days to over 4 months. These upper circulation patterns also do not exhibit a seasonal cycle. The dynamic pressure fields in Fig. 10 are averaged over the same time intervals as those for the upper layer (Fig. 3 in their paper). Intriguing connections between the upper and lower fields are suggested. For example, when the entire upper basin is filled with warm water (pattern T1), low pressure covers most of the deep basin and strong gradients exist. Conversely, when the EKWC is absent and the upper layer is mostly cold, higher pressure and weaker gradients occur at depth (pattern 3). A thorough examination of the coupling between the upper and lower layers, however, is beyond the scope of this paper.

8. Conclusions

For the first time, the deep circulation of the Ulleung Basin has been monitored by an extensive array of in situ measurements. Mean flow vectors define stable estimates of a cyclonic circulation in the UB over the 2-year measurement period. Maps of the deep streamfunction show that the cyclonic circulation consists of two cells with a ridge of higher pressure separating them. A region of high pressure and anticyclonic flow is always present around Ulleung Island. While the two annual means are similar, the quarterly means exhibit considerable differences. However, there is no evidence of a seasonal pattern in the circulation. Deep flow enters the UB through the UIG (the channel between Ulleung and Dok Islands) and along the Korean shelf break. Flow out of the basin is observed over the Korea Plateau. Outflow is also hypothesized along the eastern side of the UB, but no measurements exist in that region.

References

Bretherton, F.P., Davis, R.E., Fandry, C.B., 1976. A technique for objective analysis and design of oceanographic experiments applied to MODE-73. Deep-Sea Research 23, 559–582.

Chang, K.-I., Hogg, N.G., Suk, M.-S., Byun, S.-K., Kim, Y.-G., Kim, K., 2002. Mean flow and variability in the southwestern East Sea. Deep-Sea Research I 49, 2261–2279.

Chaplin, G., Watts, D.R., 1984. Inverted echo sounder development. IEEE Oceans '84 Proceedings 1, 249–253.

Cho, Y.K., Kim, K., 1995. Two modes of the salinity minimum layer water in the Ulleung Basin. La mer 33, 33–40.

Choi, Y.-K., 1996. Open-ocean convection in the Japan (East) Sea. La mer 34, 259–272.

Choi, B.H., 1999. Digital Atlas for Neighboring Seas of Korean Peninsula. Laboratory for Coastal And Ocean Dynamics Studies, Sung Kyun Kwan University, CDROM.

Hellerman, S., Rosenstein, M., 1983. Normal monthly wind stress over the world ocean with error estimates. Journal of Physical Oceanography 13, 1093–1104.

Hogan, P.J., Hurlburt, H.E., 2000. Impact of upper ocean-topographical coupling and isopycnal outcropping in

Japan/East Sea models with 1/8° to 1/64° resolution. Journal of Physical Oceanography 30 (10), 2535–2561.

Hurlburt, H.E., Thompson, J.D., 1980. A numerical study of loop current intrusions and eddy shedding. Journal of Physical Oceanography 10, 1611–1651.

Kim, K., Kim, K.-R., Chung, J.-Y., Yoo, H.-S., Park, S.-G., 1991. Characteristics of physical properties in the Ulleung Basin. Journal of Oceanological Society of Korea 26, 83–100.

Lie, H.-J., Suk, M.-S., Kim, C.H., 1989. Observations of southeastward deep currents off the east coast of Korea. Journal of the Oceanological Society of Korea 24, 63–68.

Mitchell, D.A., Watts, D.R., Wimbush, M., Tracey, K.L., Teague, W.J., Book, J.W., Chang, K.I., Suk, M.-S., Yoon, J.-H., 2005. Observed upper circulation patterns in the Ulleung Basin. Deep-Sea Research II, this issue [doi:10.1016/j.dsr2.2003.09.005].

Nanniti, T., Akamatsu, H., Yasuoka, T., 1966. A deep current measurement in the Japan Sea. The Oceanography Magazine 18, 63–71.

Park, J.-H., Watts, D.R., 2005, Response of the Southwestern Japan/East Sea to the atmospheric pressure. Deep-Sea Research II, this issue [doi:10.1016/j.dsr2.2003.08.007].

Paros, J.M., 1976. Digital pressure transducers. Measurements and Data 10, 74–79.

Preller, R.H., Hogan, P.J., 1998. Oceanography of the Sea of Okhotsk and the Japan/East Sea. In: Robinson, A.R., Brink, K.H. (Eds.), The Sea, vol. 11. Wiley, NY, pp. 429–481.

Senjyu, T., Sudo, H., 1993. Water characteristics and circulation of the upper portion of the Japan Sea proper water. Journal of Marine Systems 4, 349–362.

Senjyu, T., Sudo, H., 1994. The upper portion of the Japan Sea proper water; its source and circulation as deduced from isopycnal analysis. Journal of Oceanography 50, 663–690.

Senjyu, T., Sudo, H., 1996. Interannual variation of the upper portion of the Japan Sea proper water. Journal of Oceanography 52, 27–42.

Seung, Y.-H., Yoon, J.-H., 1995. Some features of winter convection in the Japan Sea. Journal of Oceanography 51, 61–73.

Shin, C.W., Byun, S.K., Kim, C., Seung, Y.H., 1998. Southward intrusion of the East Sea intermediate water into the Ulleung Basin: observations in 1992 and 1993. Journal of Korean Society of Oceanography 33, 146–156.

Takematsu, M., Nagano, Z., Ostrovskii, A.G., Kim, K., Volkov, Y., 1999. Direct measurements of deep currents in the northern Japan Sea. Journal of Oceanography 55, 207–216.

Teague, W.J., Jacobs, G.A., Perkins, H.T., Book, J.W., Chang, K.-I., Suk, M.-S., 2002. Low frequency current observations in the Korea Strait. Journal of Physical Oceanography 1621–1641.

Vasilev, A.S., Makashin, V.P., 1992. Ventilation of the Japan Sea waters in winter. La mer 30, 169–177.

Wallcraft, A.J., 1991. The Navy layered Ocean model users guide. NOARL Rep. 35, Naval Research Laboratory, Stennis Space Center, MS, 21pp. [Available from Naval Research Laboratory, Stennis Space Center, MS, 39529.]

Watts, D.R., Kontoyiannis, H., 1990. Deep-ocean bottom pressure measurement: drift removal and performance. Journal of Atmospheric and Oceanic Technology 7, 296–306.

Watts, D.R., Qian, X., Tracey, K.L., 2001. Mapping abyssal current and pressure fields under the meandering Gulf Stream. Journal of Atmospheric and Oceanic Technology 18, 1052–1067.

Wearn, R.B., Larson, N.G., 1982. Measurements of the sensitivities and drift of Digiquartz pressure sensors. Deep-Sea Research 29, 111–134.